

Numerical Testing by a Transfer-Matrix Technique of Simmons' Equation for the Local Current Density in Metal-Vacuum-Metal Junctions

Alexandre Mayer^a, Marwan S. Mousa^b, Mark J. Hagmann^c
and Richard G. Forbes^d

^a Department of Physics, University of Namur, Rue de Bruxelles 61, 5000 Namur, Belgium.

^b Department of Physics, Mutah University, Al-Karak 61710, Jordan.

^c Department of Electrical and Computer Engineering, University of Utah, Salt Lake City, Utah, USA.

^d Advanced Technology Institute, University of Surrey, Guildford GU2 7XH, United Kingdom.

Received on: 3/7/2018;

Accepted on: 8/10/2018

Abstract: We test the consistency with which Simmons' model can predict the local current density obtained for flat metal-vacuum-metal junctions. The image potential energy used in Simmons' original papers had a missing factor of 1/2. Beside this technical issue, Simmons' model relies on a mean-barrier approximation for electron transmission through the potential-energy barrier between the metals. In order to test Simmons' expression for the local current density when the correct image potential energy is included, we compare the results of this expression with those provided by a transfer-matrix technique. We also consider the current densities provided by a numerical integration of the transmission probability obtained with the WKB approximation and Simmons' mean-barrier approximation. The comparison between these different models shows that Simmons' expression for the local current density actually provides results that are in good agreement with those provided by the transfer-matrix technique, for a range of conditions of practical interest. We show that Simmons' model provides good results in the linear and field-emission regimes of current density *versus* voltage plots. It loses its applicability when the top of the potential-energy barrier drops below the Fermi level of the emitting metal.

Keywords: Field Electron Emission, Theory, Metal-Vacuum-Metal Junction, Transmission Probability, Mean-Barrier Approximation, Transfer-Matrix Technique.

PACS: 85.30.Kk, 79.70.+q, 03.65.Nk.

I. Introduction

Analytical models are extremely useful for the study of field electron emission. They provide indicative formulae for the emission current achieved with given physical parameters. This enables quantitative understanding of the role of these parameters. Analytical models also support the extraction of useful information from experimental data. They certainly guide the development of

technologies. These analytical models depend however on a series of approximations, typically the WKB (JWKB) approximation for the transmission of electrons through a potential-energy barrier [1–4]. It is therefore natural to question the accuracy of these models.

The accuracy with which the Murphy-Good formulation of Fowler-Nordheim theory [5–8] actually accounts for field electron emission from a flat metal surface was investigated in previous work [9–13]. The approach adopted by Mayer consists of comparing the results of this analytical model with those provided by a transfer-matrix technique [11–14]. This technique provides exact solutions of Schrödinger's equation for this field-emission process. The comparison with the Murphy-Good expression $J_{\text{MG}} = (\pi k_{\text{B}} T / d) / \sin\left(\frac{\pi k_{\text{B}} T}{a}\right) \times at_{\text{F}}^{-2} \Phi^{-1} F^2 \exp\left[-bv_{\text{F}} \Phi^{\frac{3}{2}} / F\right]$ for the current density obtained with an applied electrostatic field F , a work function Φ and a temperature T revealed that the results of this analytical model are essentially correct, within a factor of the order 0.5-1. In the Murphy-Good expression, $a = 1.541434 \times 10^{-6} \text{ A eV V}^{-2}$, $b = 6.830890 \text{ eV}^{-3/2} \text{ V nm}^{-1}$ [10], k_{B} is Boltzmann's constant, t_{F} and v_{F} are particular values of well-known special mathematical functions that account for the image interaction [7, 15], $d = \hbar e F / (2t_{\text{F}} \sqrt{2m\Phi})$ with e the elementary positive charge and m the electron mass. \hbar is Planck's constant $h/2\pi$. This study enabled the determination of a correction factor λ_{MG} to use with the Murphy-Good expression in order to get an exact result [13].

The objective of the present work is to apply the same approach to the analytical model developed by Simmons for the local current density through flat metal-vacuum-metal junctions [16–20]. Simmons' original model is widely cited in the literature. It was however noted that the image potential energy used in the original papers missed out a factor of $1/2$ [18, 21]. An error in the current density obtained for a triangular barrier in the low-voltage range (Eq. 25 of Ref. 16) was also mentioned [20]. Beside these technical issues, Simmons' original model relies on a mean-barrier approximation for the transmission of electrons through the potential-energy barrier in the junction. It is natural to question this approximation and test the accuracy of the equation proposed by Simmons for the current density obtained in flat metal-vacuum-metal junctions when the correct image potential energy is included. We use for this purpose the

transfer-matrix technique, since it provides exact solutions for this barrier model. This work aims to provide a useful update and a numerical validation of Simmons' model.

This article is organized as follows. In Sec. II, we present the transfer-matrix technique that is used as reference model for the quantum-mechanical simulation of metal-vacuum-metal junctions. In Sec. III, we present the main ideas of Simmons' theory. This presentation essentially focusses on the results that are discussed in this work. In Sec. IV, we compare the results of different models for the current density obtained in flat metal-vacuum-metal junctions. We finally conclude this work in Sec. V.

II. Modeling of Metal-Vacuum-Metal Junctions by a Transfer-Matrix Technique

The metal-vacuum-metal junction considered in this work is represented in Fig. 1. For this particular example, a static voltage V of 5 V is applied between the two metals. These metals have a Fermi energy ε_{F} of 10 eV and a common work function Φ of 4.5 eV. The gap spacing D between the two metals is 2 nm. We refer by μ_{I} to the Fermi level of the left-side metal (Region I). The Fermi level of the right-side metal (Region III) is then given by $\mu_{\text{III}} = \mu_{\text{I}} - eV$, where e refers to the elementary positive charge. For convenience, when presenting Simmons' theory, we will use the Fermi level μ_{I} of the left-side metal as reference (zero value) for all potential-energy values discussed in this work. The total electron energy E will also be defined with respect to μ_{I} . We will only consider positive values for the applied voltage V , so that the net electron current will always flow from the left to the right. The potential energy in Regions I and III is then given by $V_{\text{I}} = \mu_{\text{I}} - \varepsilon_{\text{F}}$ and $V_{\text{III}} = \mu_{\text{I}} - eV - \varepsilon_{\text{F}}$. The potential energy in the vacuum gap ($0 \leq z \leq D$) is given by $V(z) = \mu_{\text{I}} + \Phi - eFz + V_{\text{image}}(z)$, where $F = V/D$ is the magnitude of the electrostatic field induced by the voltage V . $V_{\text{image}}(z)$ refers to the image potential energy that applies to an electron situated between two flat metallic surfaces (see Eq. 7 in Sec. III). This vacuum region is also referred to as Region II.

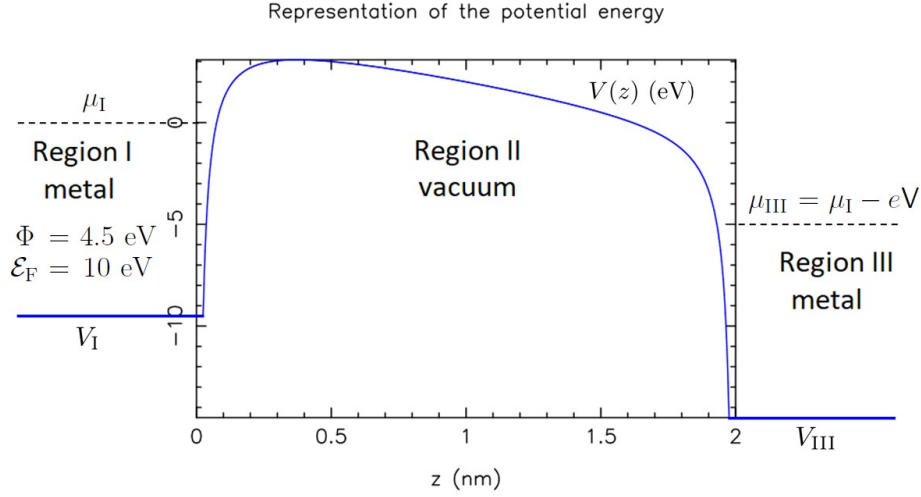


FIG. 1. Potential energy in a metal-vacuum-metal junction. A static voltage V of 5 V is applied. The gap spacing D is 2 nm. We take for convenience the Fermi level μ_I of the left-side metal as reference for the potential-energy values.

In order to establish scattering solutions in cartesian coordinates, we assume that the wave functions are periodic along the lateral x and y directions (these directions are parallel to the flat surface of the two metals). We take a lateral periodicity L of 10 nm for the wave functions (this value is sufficiently large to make our results independent of L). The boundary states in Region I and III are given respectively by:

$$\Psi_{i,j}^{I,\pm}(\vec{r}, t) = e^{i(k_{x,i}x + k_{y,j}y)} e^{\pm i \sqrt{\frac{2m}{\hbar^2}(E - V_I) - k_{x,i}^2 - k_{y,j}^2} z} e^{-iEt/\hbar} \quad \text{and}$$

$$\Psi_{i,j}^{III,\pm}(\vec{r}, t) = e^{i(k_{x,i}x + k_{y,j}y)} e^{\pm i \sqrt{\frac{2m}{\hbar^2}(E - V_{III}) - k_{x,i}^2 - k_{y,j}^2} z} e^{-iEt/\hbar},$$

where $i = \sqrt{-1}$ and the \pm signs refer to the propagation direction of these boundary states relative to the z -axis. E is the total electron energy. $k_{x,i} = i \frac{2\pi}{L}$ and $k_{y,j} = j \frac{2\pi}{L}$ are the lateral components of the wavevector (i and j are two integers also used to enumerate the boundary states). $E_z = E - \frac{\hbar^2}{2m}(k_{x,i}^2 + k_{y,j}^2)$ corresponds to the normal component of the electron energy.

By using a transfer-matrix technique, we can establish scattering solutions of Schrödinger's equation $\left[\frac{\hbar^2}{2m} \Delta + V(\vec{r}) \right] \Psi(\vec{r}, t) = i\hbar \frac{\partial}{\partial t} \Psi(\vec{r}, t)$. The idea consists of propagating the boundary states $\Psi_{i,j}^{III,\pm}$ of Region III across the vacuum gap (Region II). Since the potential energy is independent of x and y , there is no

coupling between states associated with different values of i or j and one can consider the propagation of these states separately. For the propagation of these states, we assume that the potential energy in Region II varies in steps of width Δz along the direction z . For each integer s ranging backwards from $D/\Delta z$ to 1, the potential energy is thus replaced by the constant value $V_s = \frac{1}{2}[V((s-1)\Delta z) + V(s\Delta z)]$. The solutions of Schrödinger's equation are then (i) simple plane waves

$$A_s e^{i \sqrt{\frac{2m}{\hbar^2}(E_z - V_s)z}} + B_s e^{-i \sqrt{\frac{2m}{\hbar^2}(E_z - V_s)z}} \quad \text{when}$$

$$E_z = E - \frac{\hbar^2}{2m}(k_{x,i}^2 + k_{y,j}^2) > V_s, \quad \text{(ii) real}$$

$$\text{exponentials} \quad A_s e^{-\sqrt{\frac{2m}{\hbar^2}(V_s - E_z)z}} +$$

$$B_s e^{\sqrt{\frac{2m}{\hbar^2}(V_s - E_z)z}} \quad \text{when } E_z < V_s \text{ or (iii) linear}$$

functions $A_s + B_s z$ when $E_z = V_s$. One can get arbitrarily close to the exact potential-energy barrier by letting $\Delta z \rightarrow 0$ (we used $\Delta z = 0.0001$ nm). The propagation of the states $\Psi_{i,j}^{III,\pm}$ across Region II is then achieved by matching continuity conditions for the wave function Ψ and its derivative $\frac{d\Psi}{dz}$ at the boundaries of each step Δz , when going backwards from $z = D$ to $z = 0$ [11]. The layer-addition algorithm presented in a previous work should be used to prevent numerical instabilities [22]. The solutions finally obtained for $z = 0$ are expressed as linear combinations of the boundary states $\Psi_{i,j}^{I,\pm}$ in Region I.

This procedure leads to the following set of solutions:

$$\widehat{\Psi}_{i,j}^+ \stackrel{z \leq 0}{\cong} T_{i,j}^{++} \Psi_{i,j}^{I,+} + T_{i,j}^{-+} \Psi_{i,j}^{I,-} \stackrel{z \geq D}{\cong} \Psi_{i,j}^{III,+}, \quad (1)$$

$$\widehat{\Psi}_{i,j}^- \stackrel{z \leq 0}{\cong} T_{i,j}^{+-} \Psi_{i,j}^{I,+} + T_{i,j}^{--} \Psi_{i,j}^{I,-} \stackrel{z \geq D}{\cong} \Psi_{i,j}^{III,-}, \quad (2)$$

where the complex numbers $T_{i,j}^{\pm\pm}$ correspond to the coefficients of these solutions in Region I.

We can then take linear combinations of these solutions in order to establish scattering solutions that correspond to single incident states $\Psi_{i,j}^{I,+}$ in Region I or $\Psi_{i,j}^{III,-}$ in Region III. These solutions will have the form

$$\Psi_{i,j}^+ \stackrel{z \leq 0}{\cong} \Psi_{i,j}^{I,+} + S_{i,j}^{-+} \Psi_{i,j}^{I,-} \stackrel{z \geq D}{\cong} S_{i,j}^{++} \Psi_{i,j}^{III,+}, \quad (3)$$

$$\Psi_{i,j}^- \stackrel{z \leq 0}{\cong} S_{i,j}^{--} \Psi_{i,j}^{I,-} \stackrel{z \geq D}{\cong} \Psi_{i,j}^{III,-} + S_{i,j}^{+-} \Psi_{i,j}^{III,+}, \quad (4)$$

where the complex numbers $S_{i,j}^{++}$ and $S_{i,j}^{-+}$ provide respectively the coefficients of the transmitted and reflected states for an incident state $\Psi_{i,j}^{I,+}$ in Region I. The complex numbers $S_{i,j}^{--}$ and $S_{i,j}^{+-}$ provide respectively the coefficients of the transmitted and reflected states for an incident state $\Psi_{i,j}^{III,-}$ in Region III. These coefficients are given by $S_{i,j}^{++} = [T_{i,j}^{++}]^{-1}$, $S_{i,j}^{-+} = T_{i,j}^{-+} [T_{i,j}^{++}]^{-1}$, $S_{i,j}^{--} = T_{i,j}^{--} - T_{i,j}^{-+} [T_{i,j}^{++}]^{-1} T_{i,j}^{+-}$ and $S_{i,j}^{+-} = -[T_{i,j}^{++}]^{-1} T_{i,j}^{+-}$.^[23]

These scattering solutions are finally used to compute the local current density J that flows from Region I to Region III. The idea consists of integrating the contribution of each incident state $\Psi_{i,j}^{I,+}$ in Region I (this provides the current-density contribution moving to the right) as well as the contribution of each incident state $\Psi_{i,j}^{III,-}$ in Region III (this provides the current-density contribution moving to the left). The net value of the current density is given by the difference between these two contributions. The detailed expression for the current density J has been established in previous work [24–26]. It is given formally by:

$$J_{\text{TM}} = \frac{1}{L^2} \frac{2e}{h} \int_{V_I}^{\infty} \sum_{i,j} f_I(E) \frac{v_{\text{III},(i,j)}}{v_{\text{I},(i,j)}} |S_{i,j}^{++}|^2 dE - \frac{1}{L^2} \frac{2e}{h} \int_{V_{\text{III}}}^{\infty} \sum_{i,j} f_{\text{III}}(E) \frac{v_{\text{I},(i,j)}}{v_{\text{III},(i,j)}} |S_{i,j}^{--}|^2 dE, \quad (5)$$

where the summations are restricted to solutions that are propagative both in Region I and Region III. This requires $E_z = E - \frac{\hbar^2}{2m}(k_{x,i}^2 + k_{y,j}^2) > \max(V_I, V_{\text{III}})$.

$v_{\text{I},(i,j)} = \frac{\hbar}{m} \sqrt{\frac{2m(E_z - V_I)}{\hbar^2}}$ and $v_{\text{III},(i,j)} = \frac{\hbar}{m} \sqrt{\frac{2m(E_z - V_{\text{III}})}{\hbar^2}}$ represent the normal component of the electron velocity in Regions I and III. $\frac{v_{\text{III},(i,j)}}{v_{\text{I},(i,j)}} |S_{i,j}^{++}|^2$ and $\frac{v_{\text{I},(i,j)}}{v_{\text{III},(i,j)}} |S_{i,j}^{--}|^2$ both represent the transmission probability D_{TM} of the potential-energy barrier in Region II, at the normal energy E_z . $f_I(E) = 1/\{1 + \exp[(E - \mu_I)/k_B T]\}$ and $f_{\text{III}}(E) = 1/\{1 + \exp[(E - \mu_{\text{III}})/k_B T]\}$ finally refer to the Fermi distributions in Regions I and III [27].

One can show mathematically that Eq. 5, with $L \gg 1$, is equivalent to:

$$J_{\text{TM}} = \int_{\max(V_I, V_{\text{III}})}^{\infty} \Delta N(E_z) D_{\text{TM}}(E_z) dE_z, \quad (6)$$

where the integration is over the normal energy E_z instead of the total energy E . $D_{\text{TM}}(E_z) = \frac{v_{\text{III},(i,j)}}{v_{\text{I},(i,j)}} |S_{i,j}^{++}|^2 = \frac{v_{\text{I},(i,j)}}{v_{\text{III},(i,j)}} |S_{i,j}^{--}|^2$ is the transmission probability of the potential-energy barrier at the normal energy E_z . $\Delta N(E_z) = N_I(E_z) - N_{\text{III}}(E_z)$, with $N_I(E_z) = \frac{4\pi m e}{h^3} k_B T \ln \left[1 + \exp\left(-\frac{E_z - \mu_I}{k_B T}\right) \right]$ and $N_{\text{III}}(E_z) = \frac{4\pi m e}{h^3} k_B T \ln \left[1 + \exp\left(-\frac{E_z - \mu_I + eV}{k_B T}\right) \right]$ represent the incident normal-energy distributions of the two metals. This expression of the local current density is more standard in the field emission community.

For the integration over E in Eq. 5 or E_z in Eq. 6, we use a step ΔE of 0.01 eV. It was checked that Eq. 5 and Eq. 6 provide identical results. A room temperature T of 300 K is assumed in this work.

III. Simmons' Model for the Current Density in Flat Metal-Vacuum-Metal Junctions

We present now the main ideas of Simmons' model for the local current density through a flat metal-vacuum-metal junction (see Fig. 1). This presentation focuses on the results that are actually required for a comparison with the transfer-matrix results.

We keep for consistency the notations introduced in the previous section.

A. Potential-Energy Barrier

The potential energy in the vacuum gap ($0 \leq z \leq D$) is given by [16]:

$$V(z) = \mu_1 + \Phi - eFz - \frac{1}{2} \frac{e^2}{4\pi\epsilon_0} \left[\frac{1}{2z} + \sum_{n=1}^{\infty} \left(\frac{nD}{(nD)^2 - z^2} - \frac{1}{nD} \right) \right], \quad (7)$$

where the last term of Eq. 7 accounts for the image potential energy $V_{\text{image}}(z)$ that applies to an electron situated between two flat metallic surfaces [28]. In Simmons' original papers [16, 17], there is a factor 1/2 missing in the image potential energy. This factor 1/2, which is included for correction in Eq. 7, comes from the self-interaction character of the image potential energy (the image charges follow automatically the displacement of the electron and work must actually only be done on the electron). This technical error was mentioned later by Simmons [18]. It was also pointed out in a paper by Miskovsky et al. [21].

In order to derive analytical expressions for the local current density, Simmons introduces a useful approximation for the image potential energy: $V_{\text{image}}(z) \cong -1.15\lambda \frac{D^2}{z(D-z)}$ [16]. The potential energy in the vacuum gap can then be approximated by:

$$V(z) = \mu_1 + \Phi - eFz - 1.15\lambda \frac{D^2}{z(D-z)}, \quad (8)$$

where $\lambda = \frac{e^2}{16\pi\epsilon_0} \frac{\ln 2}{D}$. We provide here a corrected expression for λ ; this includes the missing factor $1/2$.

B. Mean-Barrier Approximation for the Transmission Probability

With $E_z = E - \frac{\hbar^2}{2m}(k_x^2 + k_y^2)$ the normal component of the energy, the probability for an electron to cross the potential-energy barrier in Region II is given, within the simple WKB approximation,[1-4] by:

$$D_{WKB} = \exp \left\{ -\frac{2\sqrt{2m}}{\hbar} \int_{z_1}^{z_2} [V(z) - E_z]^{1/2} dz \right\}, \quad (9)$$

where z_1 and z_2 are the classical turning points of the barrier at the normal energy E_z (i.e., the solutions of $V(z_1) = V(z_2) = E_z$ with $z_1 \leq z_2$). Simmons then replaces $V(z)$ by $V(z)$

$= \mu_1 + \phi(z)$, where $\phi(z) = \Phi - eFz + V_{\text{image}}(z)$ represents the difference between $V(z)$ and the Fermi level μ_1 of the left-side metal (this is the metal that actually emits electrons for a positive voltage). He finally proposes a mean-barrier approximation for the transmission probability [16]:

$$D_{\text{Sim}} = \exp \left\{ -\frac{2\sqrt{2m}}{\hbar} \beta \Delta z [\bar{\phi} - (E_z - \mu_1)]^{1/2} \right\}, \quad (10)$$

where $\Delta z = z_2 - z_1$ represents here the width of the barrier at the Fermi level of the left-side metal (i.e., for $E_z = \mu_1$). $\bar{\phi} = \frac{1}{z_2 - z_1} \int_{z_1}^{z_2} \phi(z) dz$ represents the mean barrier height above the Fermi level of the left-side metal. β is a correction factor related to the mean-square deviation of $\phi(z)$ with respect to $\bar{\phi}$ [16]. For the barrier shown in Eq. 7 (image potential energy included), Simmons recommends using $\beta = 1$. The mathematical justification of Eq. 10 can be found in the Appendix of Ref. 16.

C. Analytical Expression for the Local Current Density

In his original paper [16], Simmons proposes a general formula for the net local current density J that flows between the two metals of the junction (see Eq. 20 of Ref. 16). The idea consists of integrating the contribution to the current density of each incident state in the two metals (the transmission of these states through the potential-energy barrier is evaluated with Eq. 10). Different analytical approximations were introduced by Simmons to achieve this result (in particular, in Eqs. 15, 16 and 18 that lead to Eq. 20 of Ref. 16; they require $\frac{2\sqrt{2m}}{\hbar} \beta \Delta z (\bar{\phi} + eV)^{1/2} \gg 1$). The temperature-dependence of the current density was established in Ref. 19. The final expression, which accounts for the temperature, is given by:

$$J_{\text{Sim}} = J_0 \times \frac{\pi B k_B T}{\sin(\pi B k_B T)} \times \left\{ \bar{\phi} \exp(-A \bar{\phi}^{1/2}) - (\bar{\phi} + eV) \exp(-A(\bar{\phi} + eV)^{1/2}) \right\}, \quad (11)$$

where $J_0 = \frac{e}{\hbar(2\pi\beta\Delta z)^2}$, $A = \frac{2\sqrt{2m}}{\hbar} \beta \Delta z$ and $B = \frac{A}{2\bar{\phi}^{1/2}}$. The term $J_0 \bar{\phi} \exp(-A \bar{\phi}^{1/2})$ accounts for the current moving to the right. The term $J_0 (\bar{\phi} + eV) \exp(-A(\bar{\phi} + eV)^{1/2})$ accounts

for the current moving to the left. The temperature-dependence is contained in the factor $\frac{\pi B k_B T}{\sin(\pi B k_B T)}$ [19, 29]. As mentioned previously, a temperature T of 300 K is considered in this work.

For a potential-energy barrier approximated by Eq. 8, Simmons provides an approximation for the classical turning points at the Fermi level of the left-side metal [16]. If $eV < \Phi$, with Φ the local work function, these turning points are given by:

$$\begin{aligned} z_1 &= 1.2\lambda D/\Phi \\ z_2 &= D[1 - 9.2\lambda/(3\Phi + 4\lambda - 2eV)] + z_1 \end{aligned} \quad (12)$$

Otherwise, if $eV \geq \Phi$, they are given by:

$$\begin{aligned} z_1 &= 1.2\lambda D/\Phi \\ z_2 &= (\Phi - 5.6\lambda) \left(\frac{D}{eV}\right). \end{aligned} \quad (13)$$

These expressions are calculated with the corrected factor $\lambda = \frac{e^2 \ln 2}{16\pi\epsilon_0 D}$. We can then compute the width $\Delta z = z_2 - z_1$ of the barrier at the Fermi level of the left-side metal as well as the mean barrier height $\bar{\phi}$ above this Fermi level ($\bar{\phi}$ represents the mean barrier height, over the range Δz , experienced by an electron tunneling with a normal energy equal to the left-side Fermi level) [16]. The result is given by:

$$\bar{\phi} = \Phi - \frac{eV(z_1+z_2)}{2D} - \frac{1.15\lambda D}{z_2-z_1} \ln \left[\frac{z_2(D-z_1)}{z_1(D-z_2)} \right]. \quad (14)$$

With Simmons' recommendation to use $\beta = 1$, we can compute each quantity in Eq. 11. This is the equation we want to test numerically by comparing its predictions with the results of the transfer-matrix technique. J_{Sim} depends on the mean-barrier approximation of the transmission probability (Eq. 10), on the analytical approximations introduced by Simmons to establish Eq. 11 and on Eqs. 12, 13 and 14 for $\Delta z = z_2 - z_1$ and $\bar{\phi}$.

D. Numerical Expressions for the Local Current Density

It is actually possible to integrate numerically the transmission probability D_{Sim} provided by Eq. 10. By analogy with the current density J_{TM} provided by the transfer-matrix formalism, the current density obtained by the numerical integration of D_{Sim} will be given by:

$$\begin{aligned} J_{\text{Sim-num}} &= \frac{1}{L^2} \frac{2e}{h} \int_{V_I}^{\infty} \sum_{i,j} f_I(E) D_{\text{Sim}}(E) \\ &\quad - \frac{\hbar^2}{2m} (k_{x,i}^2 + k_{y,j}^2) dE \\ &\quad - \frac{1}{L^2} \frac{2e}{h} \int_{V_{\text{III}}}^{\infty} \sum_{i,j} f_{\text{III}}(E) D_{\text{Sim}}(E) \\ &\quad - \frac{\hbar^2}{2m} (k_{x,i}^2 + k_{y,j}^2) dE \end{aligned} \quad (15)$$

$$= \int_{\max(V_I, V_{\text{III}})}^{\infty} \Delta N(E_z) D_{\text{Sim}}(E_z) dE_z \quad (16)$$

in the standard formulation. D_{Sim} is obtained here by a numerical evaluation of Eq. 10 ($\Delta z = z_2 - z_1$ and $\bar{\phi}$ are evaluated on the exact barrier given in Eq. 7). The comparison of $J_{\text{Sim-num}}$ with the results of Eq. 11 will validate the approximations that lead to this analytical expression.

It will also be interesting to consider the current density obtained by a numerical integration of the transmission probability provided by the simple WKB approximation (Eq. 9). The result will be given by:

$$\begin{aligned} J_{\text{WKB}} &= \frac{1}{L^2} \frac{2e}{h} \int_{V_I}^{\infty} \sum_{i,j} f_I(E) D_{\text{WKB}}(E) \\ &\quad - \frac{\hbar^2}{2m} (k_{x,i}^2 + k_{y,j}^2) dE \\ &\quad - \frac{1}{L^2} \frac{2e}{h} \int_{V_{\text{III}}}^{\infty} \sum_{i,j} f_{\text{III}}(E) D_{\text{WKB}}(E) \\ &\quad - \frac{\hbar^2}{2m} (k_{x,i}^2 + k_{y,j}^2) dE \end{aligned} \quad (17)$$

$$= \int_{\max(V_I, V_{\text{III}})}^{\infty} \Delta N(E_z) D_{\text{WKB}}(E_z) dE_z \quad (18)$$

in the standard formulation. J_{WKB} will enable a useful comparison with Simmons' theory given the fact that the transmission probability used by Simmons is actually an approximation of the WKB expression.

IV. Comparison between Different Models for the Local Current Density

We can compare at this point the local current densities provided by the transfer-matrix technique (J_{TM} by Eq. 5 or Eq. 6), Simmons' analytical expression (J_{Sim} by Eq.

11), a numerical integration of Simmons' formula for the transmission probability ($J_{\text{Sim-num}}$ by Eq. 16) and a numerical integration of the transmission probability provided by the WKB approximation (J_{WKB} by Eq. 18).

In order to understand the different regimes that appear in typical J - V plots, we will start by showing the dJ/dE distributions obtained for a few representative cases. This will illustrate the "linear regime" and the "field-emission regime" that are indeed appropriately described by Simmons' equation 11. In the "linear regime", the difference $\mu_I - \mu_{\text{III}}$ between the Fermi level of the two metals is smaller than the width of the total-energy distribution of the right-flowing and left-flowing contributions to the current. These two contributions tend to cancel out except in an energy window of the order of $\mu_I - \mu_{\text{III}}$, which is equal to eV . In the "field-emission regime", the Fermi level μ_{III} of the right metal is sufficiently far below μ_I to make the contribution of the left-flowing current negligible. The diode current is essentially determined by the right-flowing current, which increases rapidly with V . The "flyover regime" will be beyond the predictive capacities of Simmons' theory. In this regime, the top V_{top} of the potential-energy barrier drops below μ_I , so that electrons at the Fermi level of the left metal can fly over the top of

this barrier, provided $E_z = E - \frac{\hbar^2}{2m}(k_x^2 + k_y^2) > V_{\text{top}}$.

We consider for the moment a gap spacing D of 2 nm and three representative values of the applied voltage V : 0.5 V, 5 V and 30 V. The potential-energy distribution $V(z)$ and the total-energy distribution of the current density dJ/dE obtained for these values of the applied voltage are represented in Figs. 2, 3 and 4. The dJ/dE distributions are calculated by the transfer-matrix technique.

With an applied voltage V of 0.5 V (Fig. 2), the Fermi level $\mu_{\text{III}} = \mu_I - eV$ of the right-side metal ("Region III") is 0.5 eV below the Fermi level μ_I of the left-side metal ("Region I"). The rightwards-moving and leftwards-moving currents in the junction cancel out except in the energy window between μ_{III} and μ_I (\pm a few $k_B T$, as a result of the effect of temperature on the electron energy distributions $f_I(E)$ and $f_{\text{III}}(E)$). The integrated net current density J that flows from left to right is 1.5×10^{-6} A/cm². We are in the "linear regime" of the J - V plot. The net current density J depends indeed essentially on the separation between μ_{III} and μ_I , which is equal to eV . The mean barrier height $\bar{\phi}$ at the Fermi level is 3.2 eV. Since $eV \ll \bar{\phi}$, Eq. 11 will predict a linear J - V dependence in this regime.

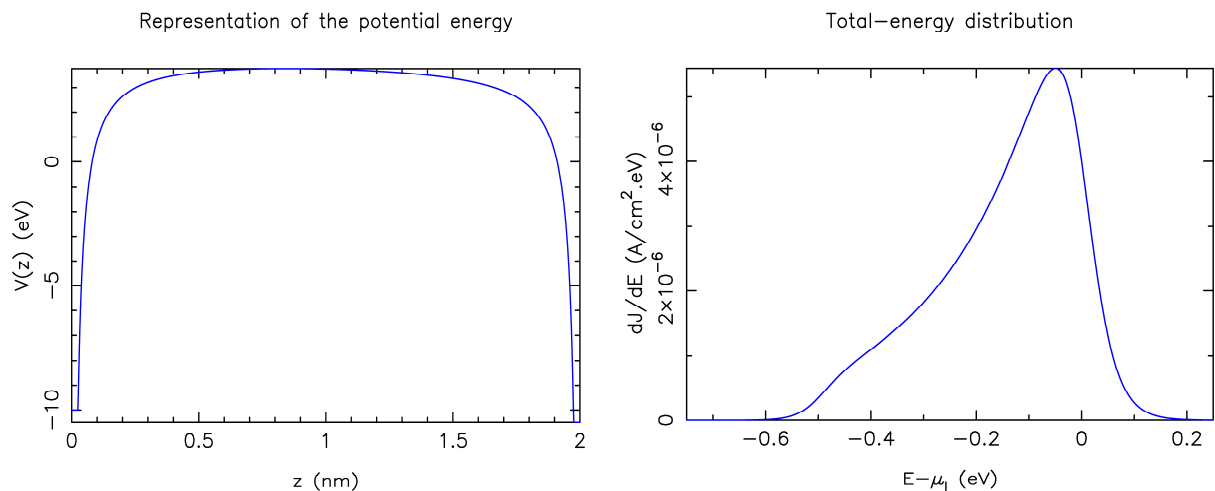


FIG. 2. Potential energy $V(z)$ (top) and total-energy distribution of the current density dJ/dE (bottom) for an applied voltage V of 0.5 V. dJ/dE is calculated by the transfer-matrix technique. We take for convenience the Fermi level μ_I of the left-side metal as reference for the potential-energy values.

With an applied voltage V of 5 V (Fig. 3), the Fermi level $\mu_{\text{III}} = \mu_{\text{I}} - eV$ of the right-side metal is 5 eV below the Fermi level μ_{I} of the left-side metal. The net current that flows through the junction is essentially determined by the right-flowing current from the left-side metal ("Region I"). The left-flowing current from the right-side metal ("Region III") only contributes for normal energies 5 eV or more below μ_{I} . Its influence on the net current is negligible. The local current density J that flows from left to right is 6.2 A/cm². The total-energy

distribution of the local current density dJ/dE (shown in Fig. 3) is a classical field-emission profile. The electrons that are emitted by the left-side metal cross the potential-energy barrier in the junction by a tunneling process. The local current density J increases rapidly with V . We are in the "field-emission regime" of the J - V plot. The mean barrier height $\bar{\phi}$ at the Fermi level is 2.6 eV in this case. Since $eV > \bar{\phi}$, Eq. 11 will predict a non-linear J - V dependence.

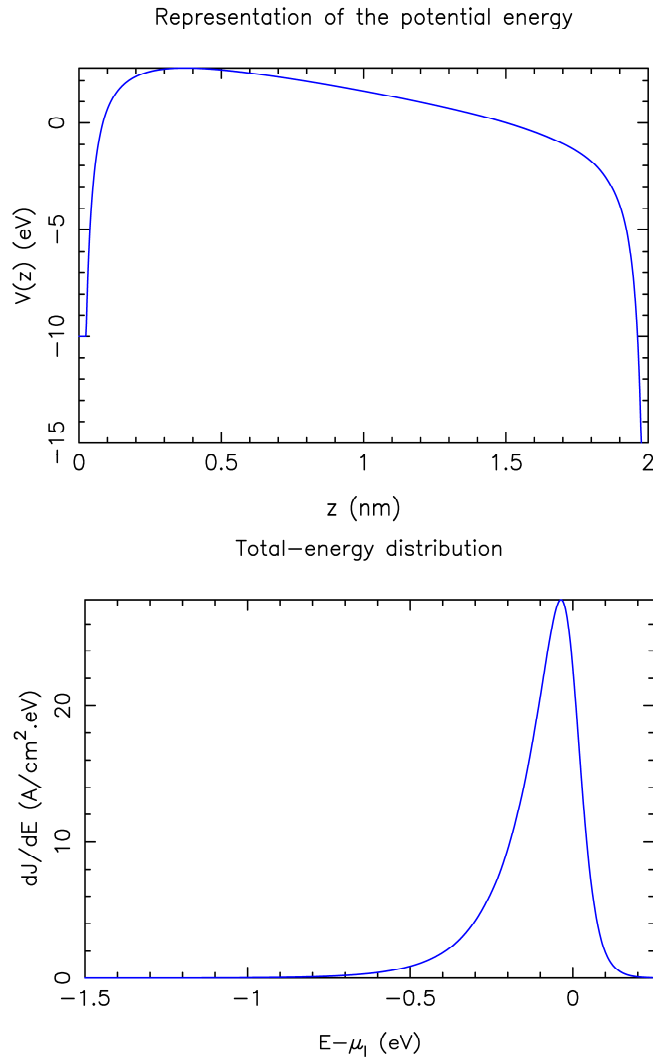


FIG. 3. Potential energy $V(z)$ (top) and total-energy distribution of the current density dJ/dE (bottom) for an applied voltage V of 5 V. dJ/dE is calculated by the transfer-matrix technique. We take for convenience the Fermi level μ_{I} of the left-side metal as reference for the potential-energy values.

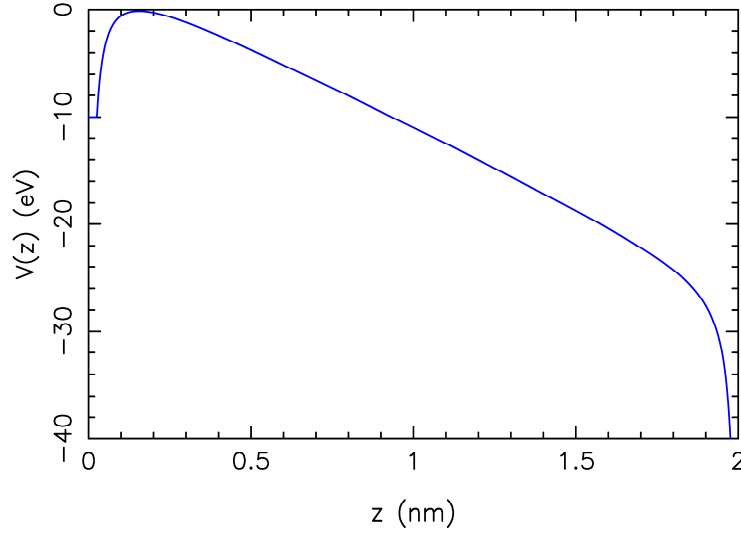
With an applied voltage V of 30 V (Fig. 4), the top V_{top} of the potential-energy barrier drops below the Fermi level μ_{I} of the left-side metal. All incident electrons with a normal energy $E_z = E - \frac{\hbar^2}{2m}(k_x^2 + k_y^2) > V_{\text{top}}$ can actually cross the junction without

tunneling, although quantum-mechanical reflection effects will occur. There is no classical turning point z_1 or z_2 at the Fermi level μ_{I} of the left-side metal and Simmons' model for the transmission probability D_{Sim} and the local current density J_{Sim} loses any

applicability. The mean barrier height $\bar{\phi}$ at the Fermi level can not be calculated in this case, since the turning points z_1 and z_2 are not defined. We are in the “flyover regime” of the J - V plot. It is probably interesting for future

work to extend Simmons' theory so that it also applies in this regime. It has been shown by Zhang that in the flyover regime, it is necessary to account for space charge effects [30].

Representation of the potential energy



Total-energy distribution

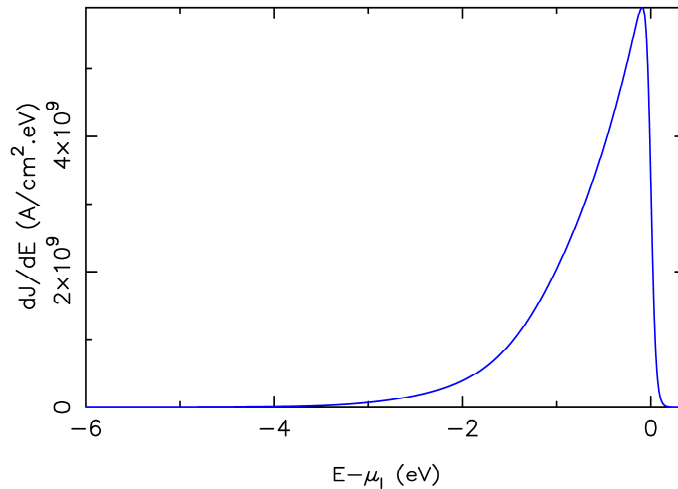


FIG. 4. Potential energy $V(z)$ (top) and total-energy distribution of the current density dJ/dE (bottom) for an applied voltage V of 30 V. dJ/dE is calculated by the transfer-matrix technique. We take for convenience the Fermi level μ_1 of the left-side metal as reference for the potential-energy values.

There is also the possibility that at very high current densities, the junction heating will be so great that junction destruction will occur. We are not aware of any work on this effect that is specifically in the context of MVM devices, but for conventional field electron emitters, it is usually thought [31, 32] that heating-related destructive effects will occur for current densities of order 10^7 to 10^8 A/cm² or higher. The situation can become

very complicated if in reality there are nanoprotusions on the emitting surface that cause local field enhancement, and hence local enhancement of the current density, or if heating due to slightly lower current densities can induce the formation and/or growth of nanoprotusions by means of thermodynamically driven electroformation processes. Detailed examination of these

heating-related issues is beyond the scope of the present work.

The J - V plot finally obtained for an applied voltage V that ranges between 0.01 V and 100 V is represented in Fig. 5. The figure represents the local current density J_{TM} obtained by the transfer-matrix technique (Eq. 5 or Eq. 6; the results are identical), the current density J_{WKB} obtained by a numerical integration of D_{WKB} (Eq. 18), the current density $J_{Sim-num}$ obtained by a numerical integration of D_{Sim} (Eq. 16) and the current density J_{Sim} provided by Simmons' analytical model (Eq. 11). These results correspond to a gap spacing D of 2 nm. The linear, field-emission and flyover regimes are clearly indicated. The results provided by the different models turn out to be in excellent agreement

up to a voltage V of 10 V. $J_{Sim-num}$ deviates progressively from the other models beyond this point. The agreement between J_{TM} , J_{WKB} and J_{Sim} is remarkable, considering the fact that the current density varies over 19 orders of magnitude for the conditions considered. Simmons' analytical model (Eq. 11) turns out to provide a very good estimate of the current density achieved in the linear and field-emission regimes. Simmons' analytical model however stops working when Eqs. 13 and 14 do not provide $\bar{\phi} \geq 0$, which is the case in the flyover regime (the top of the potential-energy barrier drops indeed below the Fermi level μ_1 of the left-side metal and Eq. 10 for the transmission probability loses any applicability).

Representation of the J - V data

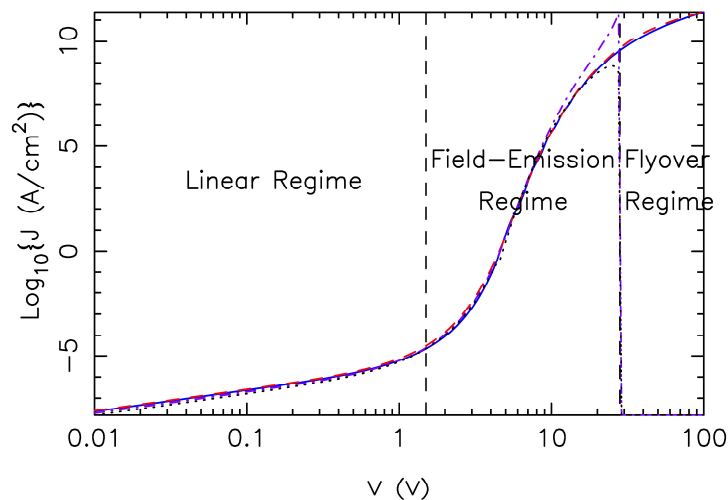


FIG. 5. J - V plot for a metal-vacuum-metal junction whose gap spacing D is 2 nm. The four curves correspond to J_{TM} (solid), J_{WKB} (dashed), $J_{Sim-num}$ (dot-dashed) and J_{Sim} (dotted). These results correspond to a common work function Φ of 4.5 eV, a Fermi energy ϵ_F of 10 eV and a temperature T of 300 K.

Fig. 6 shows more clearly the differences between the different models. This figure presents the ratios J_{WKB}/J_{TM} , $J_{Sim-num}/J_{TM}$ and J_{Sim}/J_{TM} between the current densities J_{WKB} , $J_{Sim-num}$ and J_{Sim} provided by Eqs. 18, 16 and 11 and the transfer-matrix result J_{TM} (Eq. 6). The figure shows that J_{WKB} , $J_{Sim-num}$ and J_{Sim} actually follow the transfer-matrix result J_{TM} within a factor of the order 0.5-2 up to an applied voltage V of 10 V. The current density J_{WKB} obtained by a numerical integration of D_{WKB} with respect to normal energy (Eq. 18) follows in general the transfer-matrix result more closely. The current density J_{Sim} derived

from Simmons' theory still provides very decent results. J_{Sim} (Eq. 11) is the analytical expression derived by Simmons (main focus of this article). J_{WKB} and $J_{Sim-num}$ require a numerical evaluation of the transmission probability (by Eq. 9 or Eq. 10) and a numerical integration of this transmission probability with respect to normal energy to finally obtain the current density. They are presented only for comparison. We note that J_{WKB} tends here to overestimate the local current densities. This behavior was already observed with the Schottky-Nordheim barrier that is relevant to field electron emission from

a flat metal, when considering normal energies in the vicinity of the Fermi level of a metal whose physical parameters are the same as those considered at this point ($\Phi = 4.5$ eV and $\varepsilon_F = 10$ eV) [11, 12]. As shown in Ref. 13, underestimation of the local current densities by the simple WKB approximation is also possible for smaller values of ε_F . We note finally that $J_{\text{Sim-num}}$ and J_{Sim} provide close results up to an applied voltage V of 10 V. This proves that the approximations that lead to J_{Sim} are reasonable up to this point. $J_{\text{Sim-num}}$, which is based on a numerical integration of

D_{Sim} , starts then over-estimating the current density. Simmons' mean-barrier approximation is actually a poor model of the transmission probability when the potential-energy barrier becomes too small (we can indeed have $E_z - \mu_1 > \bar{\phi}$ for values of E_z that have a non-negligible $\Delta N(E_z)$, while in reality $E_z - \mu_1 < \phi(z)$ in the potential-energy barrier). Simmons' analytical expression for the local current density (J_{Sim} by Eq. 11) appears to be more robust in these conditions. $J_{\text{Sim-num}}$ and J_{Sim} can not be applied in the flyover regime.

WKB & Simmons formulas vs Transfer Matrix

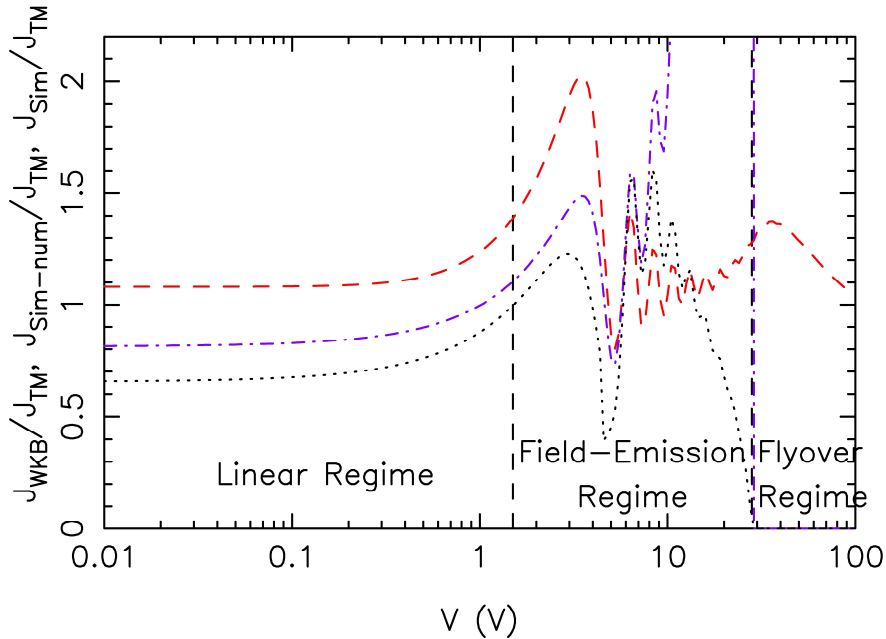


FIG. 6. Ratio $J_{\text{WKB}}/J_{\text{TM}}$ (dashed), $J_{\text{Sim-num}}/J_{\text{TM}}$ (dot-dashed) and $J_{\text{Sim}}/J_{\text{TM}}$ (dotted) for a metal-vacuum-metal junction whose gap spacing D is 2 nm. These results correspond to a common work function Φ of 4.5 eV, a Fermi energy ε_F of 10 eV and a temperature T of 300 K.

We finally provide in Table 1 a more systematic study of the ratio $J_{\text{Sim}}/J_{\text{TM}}$ between the current density J_{Sim} provided by Simmons' analytical model (Eq. 11) and the current density J_{TM} provided by the transfer-matrix technique (Eq. 6). These $J_{\text{Sim}}/J_{\text{TM}}$ ratios are calculated for different values of the gap spacing D , work function Φ and applied voltage V . The values considered for D (0.5, 1, 2 and 5 nm), Φ (1.5, 2, ... 5 eV) and V (0.01, 0.1, 1 and 10 V) are of practical interest when applying Simmons' theory for the current density in metal-vacuum-metal junctions. The results show that Simmons' analytical expression for the local current density actually provides results that are in good

agreement with those provided by the transfer-matrix technique. The factor $J_{\text{Sim}}/J_{\text{TM}}$ that expresses the difference between the two models is of the order 0.3-3.7 in most cases. Simmons' model obviously loses its applicability when Eq. 14 for $\bar{\phi}$ predicts a mean barrier height at the left-side Fermi level $\bar{\phi} < 0$. In conditions for which $\bar{\phi} \geq 0$, Simmons' analytical expression (Eq. 11) turns out to provide decent estimations of the current density J that flows in the metal-vacuum-metal junction considered in this work. This justifies the use of Simmons' model for these systems.

TABLE 1. Ratio $J_{\text{Sim}}/J_{\text{TM}}$ between the local current density J_{Sim} provided by Simmons' analytical model and the current density J_{TM} provided by the transfer-matrix technique, for different values of the gap spacing D , the common metal work function Φ and the applied voltage V . The Fermi energy ε_{F} is 10 eV and the temperature T is 300 K.

$D=0.5$ nm				
Φ (eV)	V=0.01 V	V=0.1 V	V=1 V	V=10 V
1.5	/	/	/	/
2.0	/	/	/	/
2.5	/	/	/	/
3.0	/	/	/	/
3.5	0.362	0.367	0.327	/
4.0	0.470	0.478	0.558	/
4.5	0.481	0.489	0.587	/
5.0	0.462	0.470	0.562	/
$D=1$ nm				
Φ (eV)	V=0.01 V	V=0.1 V	V=1 V	V=10 V
1.5	0.872	0.871	/	/
2.0	1.811	1.898	2.605	/
2.5	1.562	1.630	2.550	/
3.0	1.265	1.312	1.969	/
3.5	1.029	1.062	1.511	/
4.0	0.852	0.876	1.189	0.088
4.5	0.721	0.739	0.964	1.494
5.0	0.622	0.635	0.802	1.993
$D=2$ nm				
Φ (eV)	V=0.01 V	V=0.1 V	V=1 V	V=10 V
1.5	2.781	3.056	3.670	/
2.0	2.137	2.297	3.604	/
2.5	1.594	1.687	2.633	/
3.0	1.218	1.275	1.893	0.961
3.5	0.962	0.999	1.409	1.205
4.0	0.784	0.809	1.092	1.482
4.5	0.656	0.674	0.877	1.259
5.0	0.563	0.576	0.726	1.097
$D=5$ nm				
Φ (eV)	V=0.01 V	V=0.1 V	V=1 V	V=10 V
1.5	1.328	1.411	0.391	/
2.0	1.384	1.500	1.349	0.683
2.5	1.080	1.150	1.362	0.847
3.0	0.851	0.895	1.118	0.814
3.5	0.689	0.717	0.897	0.700
4.0	0.572	0.592	0.731	0.565
4.5	0.487	0.501	0.608	0.434
5.0	0.423	0.434	0.518	0.310

It has been assumed in this modeling paper that both electrodes are smooth, flat and planar. This may not be an adequate modeling approximation and it may be that in some real devices, the electrostatic field near the emitting electrode varies somewhat across the electrode surface. In such cases, the “real average current density” is probably better expressed as $J_{av} = \alpha_n J_{local}$, where J_{local} is the local current density at a typical hot spot and the parameter α_n (called here the “notional area efficiency”) is a measure of the apparent fraction of the electrode area that is contributing significantly to the current flow. However, there is no good present knowledge of the values of either of these quantities. It is also necessary to be aware that smooth-surface conceptual models disregard the existence of atoms and do not attempt to evaluate the role that atomic-level wave-functions play in the physics of tunneling. In the context of field electron emission [33–35], it is known that these smooth-surface models are unrealistic and that the neglect of atomic-level effects creates uncertainty over the predictions of the smooth-surface models. At present, it is considered that the derivation of accurate atomic-level theory is a very difficult problem, so reliable assessment of the error in the smooth-surface models is not possible at present. However, in the context of field electron emission, our present guess is that the smooth-surface models may over-predict by a factor of up to 100 or more, or under-predict by a factor of up to 10 or more. Recent results obtained by Lepetit are consistent with these estimations [36]. Uncertainties of this general kind will also apply to the Simmons' results and to the results derived in this paper.

V. Conclusions

We used a transfer-matrix technique to test the consistency with which Simmons' analytical model actually predicts the local current density J that flows in flat metal-vacuum-metal junctions. Simmons' analytical model relies on a mean-barrier approximation for the transmission probability. This enables the derivation of an analytical expression for the current density. In Simmons' original papers, there is a missing factor of 1/2 in the image potential energy. This factor was included for correction in our presentation of

Simmons' theory. We then compared the current density J_{Sim} provided by this analytical model with the current density J_{TM} provided by a transfer-matrix technique. We also considered the current densities provided by a numerical integration of the transmission probability obtained with the WKB approximation and Simmons' mean-barrier approximation. The comparison between these different models shows that Simmons' analytical model for the current density provides results that are in good agreement with an exact solution of Schrödinger's equation for a range of conditions of practical interest. The ratio J_{Sim}/J_{TM} used to measure the accuracy of Simmons' model takes values of the order 0.3-3.7 in most cases, for the conditions considered in this work. Simmons' model can obviously only be used when the mean-barrier height at the Fermi level $\bar{\Phi}$ is positive. This corresponds to the linear and field-emission regimes of J - V plots. Future work may extend the range of conditions considered for this numerical testing of Simmons' model and seek establishing a correction factor to use with Simmons' equation in order to get more exact results.

Acknowledgments

Alexandre Mayer is funded by the Fund for Scientific Research (F.R.S.-FNRS) of Belgium. He is member of NaXys, Namur Institute for Complex Systems, University of Namur, Belgium. This research used resources of the “Plateforme Technologique de Calcul Intensif (PTCI)” (<http://www.ptci.unamur.be>) located at the University of Namur, Belgium, which is supported by the F.R.S.-FNRS under the convention No. 2.5020.11. The PTCI is member of the “Consortium des Equipements de Calcul Intensif (CECI)” (<http://www.cecihpc.be>).

References

- [1] Jeffreys, H., Proc. London Math. Soc., s2-23 (1925) 428.
- [2] Wentzel, G., Z. Phys., 38 (1926) 518.
- [3] Kramers, H. A., Z. Phys., 39 (1926) 828.
- [4] Brillouin, L., Compt. Rend., 183 (1926) 24.
- [5] Fowler, R.H. and Nordheim, L., Proc. R. Soc. London Ser. A, 119 (1928) 173.
- [6] Murphy, E.L. and Good, R.H., Phys. Rev., 102 (1956) 1464.
- [7] Good, R.H. and Müller, E.W., “Handbuch der Physik” (Springer Verlag, Berlin, 1956), p176.
- [8] Young, R.D., Phys. Rev., 113 (1959) 110.
- [9] Forbes, R.G., J. Appl. Phys., 103 (2008) 114911.
- [10] Forbes, R.G., J. Vac. Sci. Technol. B, 26 (2008) 788.
- [11] Mayer, A., J. Phys. Condens. Matter, 22 (2010) 175007.
- [12] Mayer, A., J. Vac. Sci. Technol. B, 28 (2010) 758.
- [13] Mayer, A., J. Vac. Sci. Technol. B, 29 (2010) 021803.
- [14] Hagmann, M.J., Int. J. Quantum Chem., 29 (1995) 289.
- [15] Forbes, R.G. and Deane, J.H.B., Proc. R. Soc. A, 463 (2007) 2907.
- [16] Simmons, J.G., J. Appl. Phys., 34 (1963) 1793.
- [17] Simmons, J.G., J. Appl. Phys., 34 (1963) 2581.
- [18] Simmons, J.G., J. Appl. Phys., 35 (1964) 2472.
- [19] Simmons, J.G., J. Appl. Phys., 35 (1964) 2655.
- [20] Matthews, N., Hagmann, M.J. and Mayer, A., J. Appl. Phys., 123 (2018) 136101.
- [21] Miskovsky, N.M., Cutler, P.H., Feuchtwang, T.E. and Lucas, A.A., Appl. Phys. A, 27 (1982) 139.
- [22] Mayer, A. and Vigneron, J.-P., Phys. Rev. E, 59 (1999) 4659.
- [23] One can check indeed that $\Psi_{i,j}^+ = \hat{\Phi}_{i,j}^+[T_{i,j}^{++}]^{-1}$ and $\Psi_{i,j}^- = \hat{\Phi}_{i,j}^- - \hat{\Phi}_{i,j}^+[T_{i,j}^{++}]^{-1}T_{i,j}^{+-}$.
- [24] Mayer, A. and Vigneron, J.-P., Phys. Rev. B, 56 (1997) 12599.
- [25] Mayer, A., Chung, M.S., Weiss, B.L., Miskovsky, N.M. and Cutler, P.H., Phys. Rev. B, 78 (2008) 205404.
- [26] Mayer, A., Chung, M.S., Lerner, P.B., Weiss, B.L., Miskovsky, N.M. and Cutler, P.H., J. Vac. Sci. Technol. B, 30 (2012) 31802.
- [27] The use of factors of the form $f_i(E)[1-f_{\text{III}}(E)]$ and $f_{\text{III}}(E)[1-f_i(E)]$ in the two terms of the current density will provide identical results when the applied voltage V is static as in this work. For oscillating voltages, the expression 5 must however be used and we consider it therefore as fundamentally more correct.
- [28] For the transfer-matrix calculations, it is the expression 7 that is actually used for $V(z)$. The fact that $V_{\text{image}}(z)$ tends to $-\infty$ when $z \rightarrow 0$ or $z \rightarrow D$ causes convergence issues when solving Schrödinger’s equation by a transfer-matrix approach. The physical reason is related to the existence of bound states in this potential energy. These bound states would be filled in the real device. One can actually question the validity of the image interaction when we are at a few Angströms only to the surface of a metal. A solution to this issue is to cut $V(z)$ at V_I when $z \rightarrow 0$ and at V_{III} when $z \rightarrow D$. This provides the barrier depicted in Fig. 1 in which there is no singularity in the potential energy when crossing the surface of each metal.
- [29] Hrach, R., Czech. J. Phys. B, 18 (1968) 402.
- [30] Zhang, P., Sci. Rep., 5 (2015) 09826.

- [31] Mesyats, G.A., Explosive Electron Emission, (URO Press, Ekaterinburg, 1998).
- [32] Fursey, G., Field Emission in Vacuum Microelectronics, (Kluwer/Plenum, New York, 2005).
- [33] Fowler, R.H. and Guggenheim, E.A., "Statistical Thermodynamics", 2nd Ed., (Cambridge Univ. Press, London, 1949).
- [34] Sommerfeld, A., "Thermodynamics and Statistical Mechanics", (Academic Press, New York, 1964).
- [35] Ziman, J.M., "Principles of the Theory of Solids", (Cambridge Univ. Press, London, 1964).
- [36] Lepetit, B., J. Appl. Phys., 122 (2017) 215105.